

# Limit on Lorentz and CPT Violation of the Bound Neutron Using a Free Precession $^3\text{He}/^{129}\text{Xe}$ Co-magnetometer

C. Gemmel,<sup>1</sup> W. Heil,<sup>1,\*</sup> S. Karpuk,<sup>1</sup> K. Lenz,<sup>1</sup> Yu. Sobolev,<sup>1</sup> K. Tullney,<sup>1</sup> M. Burghoff,<sup>2</sup> W. Kilian,<sup>2</sup> S. Knappe-Grüneberg,<sup>2</sup> W. Müller,<sup>2</sup> A. Schnabel,<sup>2</sup> F. Seifert,<sup>2</sup> L. Trahms,<sup>2</sup> and U. Schmidt<sup>3</sup>

<sup>1</sup>*Institut für Physik, Johannes Gutenberg-Universität, 55099 Mainz, Germany*

<sup>2</sup>*Physikalische-Technische-Bundesanstalt Berlin, 10587 Berlin, Germany*

<sup>3</sup>*Physikalisches Institut, Universität Heidelberg, 69120 Heidelberg, Germany*

(Dated: November 11, 2019)

We report on the search for Lorentz violating sidereal variations of the frequency difference of co-located spin-species while the Earth and hence the laboratory reference frame rotates with respect to a relic background field. The co-magnetometer used is based on the detection of freely precessing nuclear spins from polarized  $^3\text{He}$  and  $^{129}\text{Xe}$  gas samples using SQUIDs as low-noise magnetic flux detectors. As result we can determine the limit for the equatorial component of the background field interacting with the spin of the bound neutron to be  $\tilde{b}_\perp^n < 3.7 \cdot 10^{-32}$  GeV (95% C.L.).

PACS numbers: 06.30.Ft, 07.55.Ge, 11.30.Cp, 11.30.Er, 04.80.Cc, 32.30.Dx, 82.56.Na

A great number of laboratory experiments has been designed to detect diminutive violations of Lorentz invariance. Among others, the Hughes-Drever-like experiments [1, 2], have been performed to search for anomalous spin coupling to an anisotropy in space using electron and nuclear spins with steadily increasing sensitivity [3–14]. Lorentz violating theories should generally predict the existence of privileged reference systems. In contrast with the situation at the end of the 19th century, we have a rather unique choice nowadays for such a "preferred inertial frame", i.e., the frame where the Cosmic Microwave Background (CMB) looks isotropic. Trying to measure an anomalous coupling of spins to a relic background field which permeates the Universe and points in a preferred direction in spacetime as a sort of New Aether wind is a modern analogue of the original Michelson-Morley experiment.

The theoretical framework presented by A. Kostelecky and colleagues parametrizes the general treatment of CPT- and Lorentz violating effects in a Standard Model Extension (SME) [15]. The SME was conceived to facilitate experimental investigations of Lorentz and CPT symmetry, given the theoretical motivation for violation of these symmetries. Although Lorentz-breaking interactions are motivated by models such as string theory [16], loop quantum gravity (LQG) [17–19], etc. (i.e., fundamental theories combining the Standard Model (SM) with gravity), the low-energy effective action appearing in the SME is independent of the underlying theory. Each term in the effective theory involves the expectation of a tensor field in the underlying theory. These terms are small due to Planck-scale suppression, and in principle are measurable in experiments. Predictions for parameters in the SME for a LQG system with a preferred frame were discussed, e.g., in Ref. [20].

The SME contains a number of possible terms that cou-

ple to the spins of SM-particles like electron, proton and nucleon (mostly bound neutron) [21]. These terms have set the most stringent limits on CPT and Lorentz violations. To determine the leading-order effects of a Lorentz violating potential  $V$ , it suffices to use a non-relativistic description for the particles involved given by [21]

$$V = -\tilde{b}_J^w \cdot \sigma_J^w \quad (\text{with: } J = X, Y, Z ; w = e, p, n) . \quad (1)$$

The most sensitive tests were performed using a  $^3\text{He}$ - $^{129}\text{Xe}$  Zeeman maser to place an upper limit on the neutron coupling to the anomalous field of

$$\tilde{b}_\perp^n = \sqrt{(\tilde{b}_X^n)^2 + (\tilde{b}_Y^n)^2} < 10^{-31} \text{ GeV} [9, 10] \text{ and, recently, by use of a K-}^3\text{He co-magnetometer whereby improving the previous limit by a factor of 30 [4]. An essential assumption in these so-called clock comparison experiments is that the anomalous field } \tilde{b}_J^w \text{ does not couple to magnetic moments but directly to the sample spins } \sigma_J^w. \text{ This direct coupling allows co-magnetometry that uses two different spin species to distinguish between a normal magnetic field and an anomalous field coupling. The co-magnetometer used for the presented measurements is based on the detection of freely spin precessing nuclear spins from polarized } ^3\text{He} \text{ and } ^{129}\text{Xe} \text{ samples gas with SQUIDs as low-noise magnetic flux detectors. Like in [9, 10], we search for sidereal variations of the frequency of co-located spin species while the Earth and hence the laboratory reference frame rotates with respect to a relic background field. The observable to trace possible tiny sidereal frequency modulations is the combination of measured Larmor frequencies given by}$$

$$\Delta\omega = \omega_{L,\text{He}} - \frac{\gamma_{\text{He}}}{\gamma_{\text{Xe}}} \cdot \omega_{L,\text{Xe}}. \quad (2)$$

By that measure the Zeeman-term is eliminated and thus any dependence on fluctuations and drifts of the magnetic field. For the  $^3\text{He}/^{129}\text{Xe}$  gyromagnetic ratios we took the literature values [22, 23] given by  $\gamma_{\text{He}}/\gamma_{\text{Xe}} = 2.75408159(20)$ .

\* Corresponding author: wheil@uni-mainz.de

The essential difference, in particular to [9, 10], is that by monitoring the free spin precession, an ultra-high sensitivity can be achieved with a clock which is almost completely decoupled from the environment. The design and operation of the two-species  $^3\text{He}/^{129}\text{Xe}$  co-magnetometer has been shown recently [24]. Briefly, in our measurements, we used a low-Tc DC-SQUID magnetometer system inside the strongly magnetically shielded room BMSR-2 at PTB [25]. A homogeneous guiding magnetic field  $B_0$  of about 400 nT was provided by one of the two square coil pairs which were arranged perpendicular to each other in order to manipulate the sample spins, e.g.,  $\pi/2$  spin-flip by non-adiabatic switching. The maximum field gradients were about 33 pT/cm. The  $^3\text{He}/^{129}\text{Xe}$  nuclear spins were polarized outside the shielding by means of optical pumping. Low-relaxation spherical glass vessels ( $R=3$  cm) were filled with the polarized  $^3\text{He}/^{129}\text{Xe}$  gases and placed directly below the Dewar as close as possible to SQUID sensors, which detect a sinusoidal change in magnetic flux due to the spin precession of the gas atoms in the glass cell. In order to obtain a high common mode rejection ratio, gradiometric sensor arrangements are commonly used. For our analysis it was sufficient to use a first-order gradiometer in order to suppress environmental disturbance fields. Nitrogen was added as buffer gas to suppress the van der Waals spin-relaxation of  $^{129}\text{Xe}$  [26]. In the regime of motional narrowing, i.e., at gas pressures of order mbar and at low magnetic fields [27, 28], transverse spin relaxation times  $T_2^*$  of up to 60 h have been measured for  $^3\text{He}$ . The actual limitation in the  $T_{2,\text{Xe}}^*$  of Xenon is given by the relatively short wall relaxation time of  $8\text{ h} < T_{1,\text{wall}}^{\text{Xe}} < 16\text{ h}$ . Therefore, the total observation time  $T$  of free spin-precession of our  $^3\text{He}/^{129}\text{Xe}$  co-magnetometer is set by this characteristic time constant. According to the Cramer-Rao Lower Bound (CRLB) [29], the accuracy by which the frequency of a damped sinusoidal signal can be determined is given by

$$\sigma_f \geq \frac{\sqrt{12}}{(2\pi) \cdot \text{SNR} \cdot \sqrt{f_{\text{BW}}} \cdot T^{3/2}} \times \sqrt{C(T, T_2^*)}. \quad (3)$$

$\text{SNR}$  denotes the signal-to-noise ratio,  $f_{\text{BW}}$  the bandwidth, and  $C(T, T_2^*)$  describes the effect of exponential damping of the signal amplitude with  $T_2^*$ . For observation times  $T \leq T_2^*$ ,  $C(T, T_2^*)$  is of order one. Deviations from the CRLB power law, due to noise sources inherent in the co-magnetometer itself did not show up in Allan standard deviation plots used to identify the power-law model for the phase noise spectrum of our runs with  $T \approx 14\text{ h}$ , typically [24].

The recorded signal is a superposition of the  $^3\text{He}$  and  $^{129}\text{Xe}$  precession signals at Larmor frequencies  $\omega_{\text{He}} = \gamma_{\text{He}} \cdot B_0 \approx 2\pi \cdot 13.4\text{ Hz}$  and  $\omega_{\text{Xe}} = \gamma_{\text{Xe}} \cdot B_0 \approx 2\pi \cdot 4.9\text{ Hz}$  as shown in FIG. 1. Analog to similar problems of data analysis [30] phases of sub-data sets were analysed: The data of each run ( $j = 1, \dots, 7$ ) were divided into sequential time intervals ( $i$ ) of  $\tau = 3.2\text{ s}$  ( $i = 1, \dots, N_j$ ). The number of obtained sub-data sets laid between 13350 <

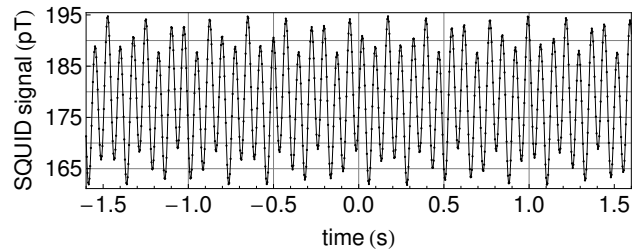


FIG. 1. Typical sub-data set of 3.2 s length showing the recorded SQUID gradiometer signal of the precessing  $^3\text{He}/^{129}\text{Xe}$  sample spins (sampling rate:  $r_s=250\text{ Hz}$ ). The error bar at each data point of  $\pm 34\text{ fT}$  is less than the symbol size. The signal amplitudes at the beginning of each run were typically  $S_{\text{He}} \approx 13\text{ pT}$  and  $S_{\text{Xe}} \approx 4\text{ pT}$ .

$N_j < 18000$  corresponding to observation times  $T_j$  of coherent spin precessions in the range of  $12\text{ h} < T_j < 16\text{ h}$ . For each sub-data set a  $\chi^2$ -minimization was performed, using the fit-function

$$A^i(t) = A_{\text{He}}^i \cdot \sin(\omega_{\text{He}}^i t) + B_{\text{He}}^i \cdot \cos(\omega_{\text{He}}^i t) + A_{\text{Xe}}^i \cdot \sin(\omega_{\text{Xe}}^i t) + B_{\text{Xe}}^i \cdot \cos(\omega_{\text{Xe}}^i t) + (c_0^i + c_{\text{lin}}^i \cdot t) \quad (4)$$

with a total of 8 fit-parameters. Within the relatively short time intervals, the term  $(c_0^i + c_{\text{lin}}^i \cdot t)$  represents the adequate parameterization of the SQUID gradiometer offset showing a small linear drift due to the elevated  $1/f$ -noise at low frequencies ( $< 1\text{ Hz}$ ) [24]. On the other hand, the chosen time intervals are long enough to have a sufficient number of data points (800) for the  $\chi^2$ -minimization. The sum of sine and cosine terms are chosen to have only linear fitting parameters for the sub-data set phases which are given by

$$\varphi^i = \arctan(B^i/A^i). \quad (5)$$

The normalized  $\chi^2$  ( $\chi^2/\text{d.o.f}$ ) of most sub-data sets ( $i$ ) is close to 1 which is consistent with the assigned error bar to each data point of  $\pm 34\text{ fT}$  (see FIG. 1). The latter value is the typical noise signal  $N_s$  derived from the mean system noise  $\bar{\rho}_s \approx 3\text{ fT}/\sqrt{\text{Hz}}$  in the recorded effective bandwidth of 100 Hz. Jumps in the SQUID signal in the order of 1 pT caused by external disturbances gave  $\chi^2/\text{d.o.f} \gg 1$  for the respective sub-data sets. In the analysis we therefore disregarded all sub-data sets with  $\chi^2/\text{d.o.f} \geq 2$  ( $< 0.5\%$  in total). For each sub-data set of chosen time interval  $-1.6\text{ s} \leq (t - t_{i-1,j}) \leq +1.6\text{ s}$  (see FIG. 1), we finally obtain numbers for the respective fit parameters  $\omega_{\text{He}}^i$ ,  $\omega_{\text{Xe}}^i$ ,  $\varphi_{\text{He}}^i$ ,  $\varphi_{\text{Xe}}^i$  including error bars. In a further step, we can deduce values for the average frequency  $\bar{\omega}^j = \frac{1}{N_j} \sum_{i=1}^{N_j} \omega^i$  for each run. The accumulated phase (omitting the index  $j$ ) is then determined to

be<sup>1</sup>

$$\Phi(t = m\tau) = \Phi(t = (m-1)\tau) + \bar{\omega} \cdot \tau + \varphi^m - \text{mod} [\Phi(t = (m-1)\tau) + \bar{\omega}\tau; 2\pi] \quad (6)$$

with  $m=1, \dots, N-1$  and  $\Phi(t=0) = \varphi^1$  being the phase offset of the first time interval. Following Eq. 2 the extracted phase difference  $\Delta\Phi^{(1)}(t) = \Phi_{\text{He}}^{(1)}(t) - (\gamma_{\text{He}}/\gamma_{\text{Xe}}) \cdot \Phi_{\text{Xe}}^{(1)}(t)$  is plotted for run (1).  $\Delta\Phi^{(1)}(t)$  is expected to be constant if there is no sidereal modulation of the spin precession frequency and/or no other drifts and noise sources. Nevertheless, in addition to an arbitrary phase offset an almost linear time dependence is seen in FIG. 2a. The dominant contribution is caused from the Earth's rotation, i.e., the rotation of the SQUID detector with respect to the precessing spins. For the location of

the PTB Berlin, Germany ( $\theta=52.5164^\circ$  north) and the angle between north-south direction and guiding magnetic field ( $\rho=28^\circ$ ), the linear term in the weighted phase difference due to Earth's rotation is given by [24]

$$\Phi_{\text{Earth}} = -\Omega_{\text{SD}} \cdot (1 - \gamma_{\text{He}}/\gamma_{\text{Xe}}) \cdot \cos \rho \cdot \cos \theta \cdot t = 6.87263 \times 10^{-5} \text{ rad/s} \cdot t \quad (7)$$

$\Omega_{\text{SD}}$  is the angular frequency of the sidereal day with  $\Omega_{\text{SD}} = 2\pi/T_{\text{SD}} = 2\pi/(23^{\text{h}} : 56^{\text{min}} : 4.091^{\text{s}})$ . Subtracting this term from  $\Delta\Phi^{(1)}(t)$ , we get the corrected phase  $\Delta\Phi_{\text{corr}}^{(1)}(t)$  which is plotted in FIG. 2a, too. Let us assume that there is no sidereal variation of the  $^3\text{He}/^{129}\text{Xe}$  frequencies induced by Lorentz-violating couplings, then  $\Delta\Phi_{\text{corr}}^{(j)}(t)$  can be described best by

$$\Phi_{\text{fit}}^{(j)}(t) = \Phi_0^{(j)} + \Delta\omega_{\text{lin}}^{(j)}(t - t_{0,j}) + E_{\text{He}}^{(j)} \cdot \exp\left(\frac{-(t - t_{0,j})}{T_{2,\text{He}}^{*(j)}}\right) + E_{\text{Xe}}^{(j)} \cdot \exp\left(\frac{-(t - t_{0,j})}{T_{2,\text{Xe}}^{*(j)}}\right). \quad (8)$$

$$\text{with } \Phi_{\text{fit}}^{(j)}(t) = \begin{cases} \Phi_{\text{fit}}^{(j)}(t) & \text{for } t_{0,j} \leq t \leq (t_{0,j} + N_j \cdot \tau) \\ 0 & \text{elsewhere} \end{cases}$$

$t_{0,j}$  is the absolute starting time of each run. Our interpretation of the terms are as follows:  $\Phi_0^{(j)}$  is a general phase offset and  $\Delta\omega_{\text{lin}}^{(j)}(t - t_{0,j})$  is an additional linear phase shift mainly arising from deviations of the gyromagnetic ratios of  $^3\text{He}$  and  $^{129}\text{Xe}$  from their literature values due to chemical shifts and uncertainties in the subtraction of  $\Phi_{\text{Earth}}$  [24]. The two exponential terms with amplitudes  $E_{\text{He}}^{(j)}$  and  $E_{\text{Xe}}^{(j)}$  reflect the respective phase shift due to demagnetization fields in a non-ideal spherical cell seen by the spin ensembles (self shift). These phase shifts are directly correlated to the decay times  $T_{2,\text{He}}^{(j)}$  and  $T_{2,\text{Xe}}^{(j)}$  of the respective signal amplitude of the precessing Helium and Xenon spins [24]. As the  $T_2^{*(j)}$  times can be determined independently for both spin species from the experiment, four fit parameters are left for each run, such that the fit model is basically a linear function in parameters.

Fitting the corrected phase difference  $\Delta\Phi_{\text{corr}}^{(j)}(t)$  to Eq. 8 and subtracting the fit function from  $\Delta\Phi_{\text{corr}}^{(j)}(t)$  results in the phase residual as shown for run (1) in FIG. 2b. Due to the exponential decay of the signal amplitudes, mainly that of Xenon with the shorter  $T_{2,\text{Xe}}^*$  of only 4 h to 5 h, the  $SNR$  decreases resulting in an increase of the residual phase noise, i.e.,  $\sigma_{\Phi,\text{res}} \propto \exp(t/T_{2,\text{Xe}}^*)$  [24].

In the last step, a piecewise fit function was defined, which is a combined fit to all seven runs, now including the parameterization of the sidereal phase modulation

$$\Phi_{\text{fit}}^{\text{SD}}(t) = \sum_{j=1}^7 \Phi_{\text{fit}}^{(j)}(t) + \{ a_s \cdot \sin(\Omega_{\text{SD}}(t - t_{0,1}) + \varphi_{\text{SD}}) - a_c \cdot \cos(\Omega_{\text{SD}}(t - t_{0,1}) + \varphi_{\text{SD}}) \} \quad (9)$$

$\varphi_{\text{SD}}$  represents the phase offset of sidereal modulation at the local sidereal time  $t_{\text{SD}} = 0.4053$  (units of sidereal day) at the beginning ( $t_{0,1}$ ) of the first run with  $\varphi_{\text{SD}} = 2\pi \cdot t_{\text{SD}}$ .

FIG. 3 shows the corrected phase differences  $\Phi_{\text{corr}}^{(j)}(t)$  together with the fit function  $\Phi_{\text{fit}}^{\text{SD}}(t)$  (white solid line) for all seven runs. The  $\chi^2/\text{d.o.f.}$  of the fit gave 1.868, which shows that the phase model of Eq. 8 may be somewhat incomplete or, what is more likely, the phase errors are underestimated in the analysis of the sub-data sets. In order to take an (unknown) uncertainty into account, the errors on the phases were scaled to obtain a  $\chi^2/\text{d.o.f.}$  of one, as recommended, e.g., by Ref. [31, 32]. In Table I (2<sup>nd</sup> row) the fit results for the amplitudes  $a_c$  and  $a_s$  of the sidereal phase modulation are shown together with their correlated and uncorrelated  $1\sigma$ -errors.

It is noticeable, that the uncorrelated error which represents the integrated measurement sensitivity of our  $^3\text{He}/^{129}\text{Xe}$  co-magnetometer is about a factor of 50 less than the correlated one. The big correlated error on  $a_s$  and  $a_c$  is caused by a piecewise similar time structure of  $\Phi_{\text{fit}}^{(j)}(t)$  and the sidereal phase modulation in the fit-function of Eq. 9. On a closer look, this can be

<sup>1</sup> As the maximal frequency deviation  $\Delta\omega$  from the mean  $\bar{\omega}^j$  was smaller than  $5 \cdot 10^{-6}$  rad/s in the course of one run [24], we had at all times  $\Delta\omega \cdot \tau \ll 2\pi$ .

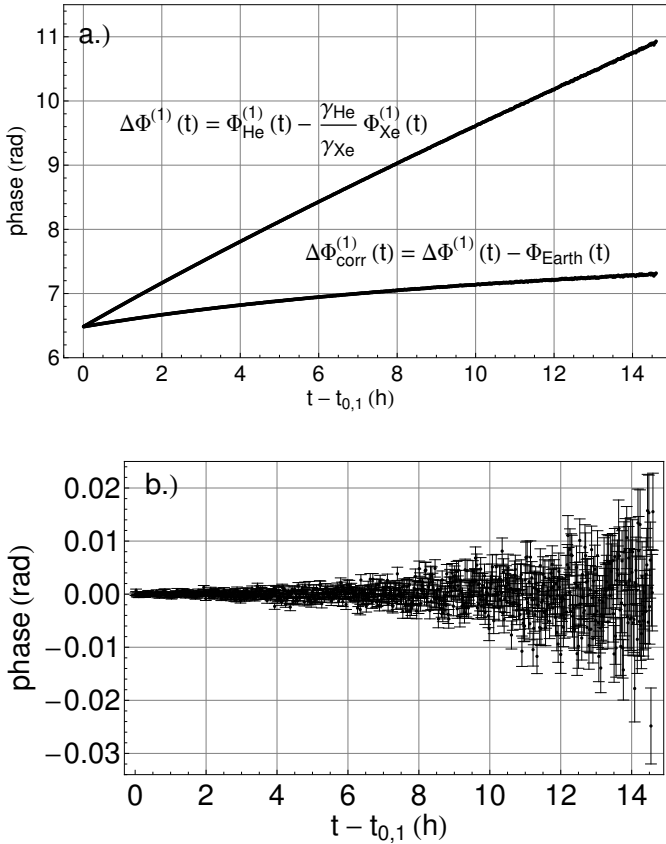


FIG. 2. (a) Measured phase differences  $\Delta\Phi^{(1)}(t)$  for run (1) and the corresponding corrected phases  $\Delta\Phi_{\text{corr}}^{(1)}(t)$  after subtraction of the effect of the Earth's rotation. (b) Phase residuals after subtraction of phase drifts given by the fit-model of Eq. 8 (one data point comprises 20 sub-data sets, i.e.,  $\Delta t = 64$  s)

traced back to the relatively short  $T_{2,\text{Xe}}^{*(j)}$ -times (compared to  $T_{\text{SD}}$ ) that enter in the argument of the exponential terms of Eq. 8. Therefore, the present sensitivity limit of our  ${}^3\text{He}/{}^{129}\text{Xe}$  co-magnetometer is set by the correlated error. In order to substantiate that more clearly, we changed the fit-model of Eq. 9 by taking multiples of  $\Omega_{\text{SD}}$  ( $\Omega'_{\text{SD}} = g \cdot \Omega_{\text{SD}}$ ), i.e., replacing  $T_{\text{SD}}$  by  $T'_{\text{SD}} = T_{\text{SD}}/g$ . The results show that the correlated error approaches the uncorrelated one already for  $g \geq 3$  (see Table I). The uncorrelated error, however, is only marginally affected by this procedure, as expected. From Table I (2<sup>nd</sup> row) we now extract the rms value of the sidereal phase

amplitude  $\Phi_{\text{SD}} = \sqrt{a_s^2 + a_c^2}$ , yielding  $(2.25 \pm 2.29)$  mrad (95% C.L.). This result is consistent with the absence of Lorentz- and CPT-violating effects, giving reasonable assumptions about the probability distribution for  $\Phi_{\text{SD}}$  [33].

In terms of the SME [21] we can express the sidereal phase amplitudes according to

$$a_s = \frac{2\pi}{\Omega_{\text{SD}}} \cdot \delta\nu_X \quad \text{and} \quad a_c = \frac{2\pi}{\Omega_{\text{SD}}} \cdot \delta\nu_Y \quad (10)$$

with  $2\pi |\delta\nu_{X,Y}| \cdot \hbar = \left| 2 \cdot (1 - \gamma_{\text{He}}/\gamma_{\text{Xe}}) \cdot \sin \chi \cdot \tilde{b}_{X,Y}^n \right|$ .  $\chi$  is the angle between the Earth's rotation axis and the quantization axis of the spins ( $\chi=57^\circ$ ). Within the Schmidt model [34], the valence neutron of  ${}^3\text{He}$  and  ${}^{129}\text{Xe}$  determines the spin and the magnetic moment of the nucleus. Thus, our  ${}^3\text{He}/{}^{129}\text{Xe}$  co-magnetometer is sensitive to the bound neutron parameters  $\tilde{b}_{X,Y}^n$ . From that, we can deduce numbers for  $\tilde{b}_{X,Y}^n$  and the corresponding value  $\tilde{b}_\perp^n = \sqrt{(\tilde{b}_X^n)^2 + (\tilde{b}_Y^n)^2}$  giving

$$\left| \tilde{b}_X^n \right| = 3.36 \pm 1.72 \cdot 10^{-32} \text{ GeV} \quad (1\sigma),$$

$$\left| \tilde{b}_Y^n \right| = 1.43 \pm 1.33 \cdot 10^{-32} \text{ GeV} \quad (1\sigma) \quad \text{and}$$

$$\tilde{b}_\perp^n = |3.65 \pm 3.72| \cdot 10^{-32} \text{ GeV} \quad (95\% \text{ C.L.}).$$

With  $\tilde{b}_\perp^n < 3.7 \cdot 10^{-32}$  GeV we have set an upper limit on neutron spin coupling to possible Lorentz and CPT violating background tensor fields. Further improvements for Lorentz and CPT tests using the free spin precession  ${}^3\text{He}/{}^{129}\text{Xe}$  co-magnetometer can be achieved via two mayor steps: First, the relatively short wall relaxation time of  ${}^{129}\text{Xe}$  limiting the total observation time  $T$  of free spin precession has to be increased considerably ( $T_{1,\text{wall}} \approx T_{\text{SD}}$ ) such that we approach the measurement sensitivity given by the uncorrelated error. Since the latter one follows the  $\propto T^{-3/2}$  power law according to CRLB of Eq. 3, the longer observation time  $T$  will lead to an additional increase in sensitivity. Second, the number of measurement runs have to be increased to a period of 100 days. Besides gain in statistics, the long time span provides an important separation between sidereal and possible diurnal variations.

This work was supported by the Deutsche Forschungsgemeinschaft (DFG) under contract number BA 3605/1-1.

- [1] V. W. Hughes and H. G. Robinson and V. Beltran-Lopez, Phys. Rev. Lett. **4** (1960) 342  
 [2] R. W. P. Drever, Philosophical Magazine **6** (1961) 683  
 [3] J. D. Prestage et al., Phys. Rev. Lett. **54** (1985) 2387

- [4] J. M. Brown et al., Phys. Rev. Lett. **105** (2010) 151604  
 [5] S. K. Lamoreaux et al., Phys. Rev. Lett. **57** (1986) 3125  
 [6] S. K. Lamoreaux et al., Phys. Rev. D **39** (1989) 1082  
 [7] T. E. Chupp et al., Phys. Rev. Lett. **63** (1989) 1541

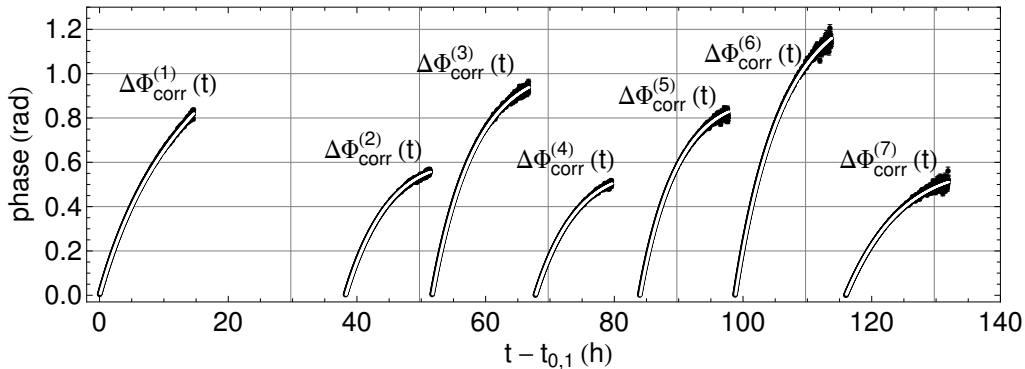


FIG. 3. Corrected phase differences  $\Delta\Phi_{\text{corr}}^{(j)}(t)$  with combined fit function  $\Phi_{\text{fit}}^{\text{SD}}(t)$  (white solid line) for the seven runs (one data point comprises 20 sub-data sets, i.e.,  $\Delta t = 64$  s). In order to present these results in a common plot, the general phase offset  $\Phi_0^{(j)}$  was subtracted from  $\Delta\Phi_{\text{corr}}^{(j)}(t)$  for each run.

	$a_c$ (mrad)	$\sigma_{a_c}^{\text{corr}}$ (mrad)	$\sigma_{a_c}^{\text{uncorr}}$ (mrad)	$a_s$ (mrad)	$\sigma_{a_s}^{\text{corr}}$ (mrad)	$\sigma_{a_s}^{\text{uncorr}}$ (mrad)
$0.5 \cdot \Omega_{\text{SD}}$	3.353	6.572	0.018	0.488	7.991	0.016
$\Omega_{\text{SD}}$	-0.882	0.814	0.015	-2.067	1.057	0.019
$2 \cdot \Omega_{\text{SD}}$	-0.048	0.120	0.016	-0.149	0.112	0.017
$3 \cdot \Omega_{\text{SD}}$	-0.184	0.052	0.019	-0.011	0.043	0.016
$4 \cdot \Omega_{\text{SD}}$	-0.001	0.034	0.018	0.057	0.030	0.016

TABLE I. Results for the sidereal phase amplitudes  $a_c$  and  $a_s$  together with their correlated and uncorrelated  $1\sigma$ -errors ( $2^{\text{nd}}$  row) determined by a  $\chi^2$ -minimization using the fit model of (Eq. 9). In order to demonstrate the strong dependence of the correlated error on the angular frequency of the sidereal day  $\Omega_{\text{SD}}$ , corresponding fit results are shown for multiples of  $\Omega_{\text{SD}}$ :  $\Omega'_{\text{SD}} = g \cdot \Omega_{\text{SD}}$ .

[8] C. J. Berglund, Phys. Rev. Lett. **75** (1995) 1879  
[9] D. Bear et al., Phys. Rev. Lett. **85** (2000) 5038  
[10] D. Bear et al., Phys. Rev. Lett. **89** (2002) 209902(E)  
[11] D. F. Phillips, Phys. Rev. D **63** (2001) 111101  
[12] F. Canè, Phys. Rev. Lett. **93** (2004) 230801  
[13] B. R. Heckel et al., Phys. Rev. D **78** (2008) 092006  
[14] I. Altarev, Phys. Rev. Lett. **103** (2009) 081602  
[15] D. Colladay and V. A. Kostelecký, Phys. Rev. D **58** (1998) 116002  
[16] J. Ellis and N. E. Mavromatos and D. V. Nanopoulos, Phys. Rev. D **63** (2000) 024024, and references therein  
[17] H. Nicolai, Class. Quantum Grav. **22** (2005) R193  
[18] R. Gambini and J. Pullin **59** (1999) 124021  
[19] P. M. Crichigno and H. Vucetich, Phys. Lett. B **651** (2007) 313

[20] H. Vucetich, arXiv:gr-qc/0502093v1 (2005)  
[21] V. A. Kostelecký and C. D. Lane, Phys. Rev. D **60** (1999) 116010  
[22] International council for Science: Committee on Data for Science and Technology (CODATA), www.codata.org (2007)  
[23] M. Pfeffer and O. Lutz, J. Magn. Res. A **106** (2005) 106  
[24] C. Gemmel et al., Eur. Phys. J. D **57** (2010) 303  
[25] J. Bork et al., Biomag. **2000** (2000) 970  
[26] B. Chann et al., Phys. Rev. Lett. **88** (2002) 113201  
[27] G. D. Cates and S. R. Schaefer and W. Happer **37** (1988) 2877  
[28] W. Kilian and F. Seifer and A. Haller **42** (2007) 197  
[29] S. M. Kay, *Fundamentals of Statistical Signal Processing: Estimation Theory (Vol. 1)*, (Prentice Hall, New Jersey, 1993)  
[30] C. D. Hoyle et al., Phys. Rev. D **70** (2004) 042004  
[31] The Particle Data Group, Phys. Lett. B **592** (2004) 14  
[32] Williams, W. H. Press and S. A. Tenkolsky and W. T. Vetterling and B. P. Flannery *Numerical Recipes 3rd Edition: The Art of Scientific Computing*, (Cambridge University Press, New York, 2007)  
[33] The probability distribution  $P$  for  $\Phi_{\text{SD}}$  is formed by multiplying the distributions for  $a_s$  and  $a_c$ , converting to polar coordinates, and integrating over the polar angle. If  $a_s$  and  $a_c$  have zero mean value and the same error  $\sigma$ , the probability distribution takes the form  $P(\delta\Phi_{\text{SD}}) = \frac{\Phi_{\text{SD}}}{\sigma^2} \cdot \exp\left(\frac{-\Phi_{\text{SD}}^2}{2\sigma^2}\right)$ . As an approximation we take the average of both errors  $\sigma = (\delta a_s + \delta a_c)/2$  and determine the 95% error by setting  $\int_0^{\delta\Phi_{\text{SD}}} P(\Phi_{\text{SD}}) d\Phi_{\text{SD}} = 0.95$  giving  $\delta\Phi_{\text{SD}} = 2.29$  mrad.  
[34] Th. Schmidt, Zeitschrift für Physik A: Hadrons and Nuclei **106** (1937) 358